AIAA SciTech Forum
8-12 January 2024, Orlando, FL
AIAA SCITECH 2024 Forum

10.2514/6.2024-2862

Numerical Studies of Ram-Air Intake for near-Earth Satellites

Nishita Ravuri*, Stephen Scully†, and Ashish Vashishtha‡
South East Technological University, Carlow Campus, Ireland R93 V960

The operation of satellites in Earth orbits with altitudes lower than 450 km involves dealing with rarefied atmosphere environment. To compensate for the aerodynamic drag present in this low-density atmosphere, satellites employ traditional Electric Propulsion, EP (limited operational life) or Air-Breathing Electric Propulsion Systems, ABEP (longer operational life). Careful geometric design of intakes of ABEP systems is critical for its performance. The main motivation of this research is 1) to understand the complex flow around basic intake configurations of ABEP systems in high-speed rarefied environment- using Direct Monte Carlo Simulation (DSMC) methods, and 2) to design compression-assisted air-breathing intake geometry operating efficiently at various orbital speeds for VLEO/SLEO satellite applications. Two-dimensional axisymmetric, time-dependent Direct Simulation Monte-carlo (DSMC) method has been utilized based on open-source SPARTA DSMC Simulator for various intake geometries at three relevant altitudes. Initial simulations of basic hollow cylinder (straight duct) geometry were run, followed by an analysis of different convergent angles for converging duct intakes, for both specular and diffuse gas-surface interactions. The results have been analysed for the collection efficiencies, mass flow rates at the entry and exit planes, drag force and the number density profiles. It was observed that with increase in altitude, there is a considerable decrease in the collection efficiencies under diffuse reflection conditions, and a considerable increase of drag coefficients under specular reflection conditions.

Nomenclature

α	=	Accommodation Coefficient
C_D	=	Drag coefficient
η_c	=	Collection Efficiency
$fnum$	=	Ratio of real-to-simulated particles
F	=	External force acting on a particle
F_D	=	Drag Force
f	=	Generic Function
h	=	Orbit Altitude
k_B	=	Boltzmann constant
Kn	=	Knudsen Number
m_{flux}	=	Mass Flux
M	=	Mach Number
$nrho$	=	Number Density
p_∞	=	Freestream Pressure
ρ_∞	=	Free-stream Density
T_∞	=	Freestream Temperature
T_w	=	Wall Temperature
v_∞	=	Free-stream Velocity

I. Introduction

The global satellite-based Earth Observation (EO) market stands for $5.1 Billion as of year 2021 and is expected to grow by more than twice the amount in the next decade (to $11.3 Billion). All EO satellites benefit from the

*Postgraduate Student, Department of Aerospace & Mechanical Engineering, SETU, Carlow Campus, IRELAND.
†Lecturer, Department of Electronics & Communication Engineering, SETU, Carlow Campus, IRELAND
‡Lecturer, Department of Aerospace & Mechanical Engineering, SETU, Carlow Campus, IRELAND and AIAA Senior Member

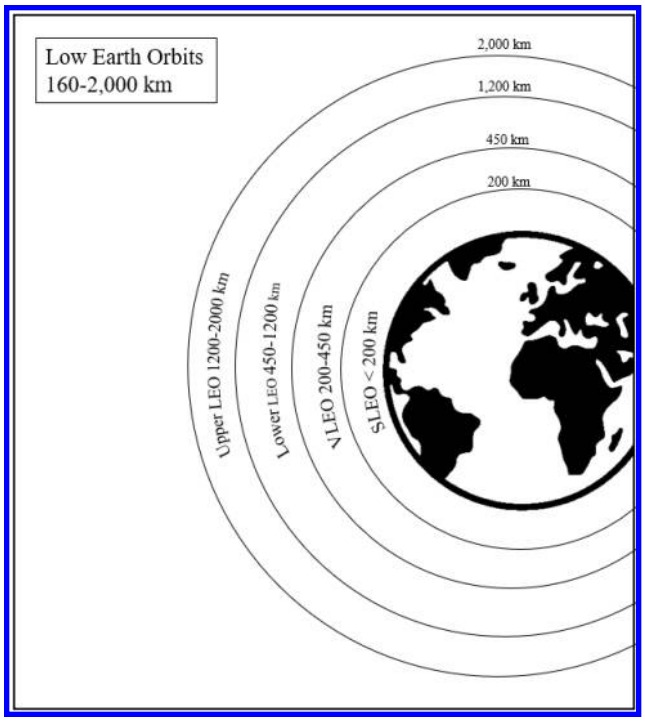

Fig. 1 Illustration of Low Earth Orbits

proximity to the earth's surface with their operation in the Low-Earth Orbits (altitude range between 400-1000 km). These orbit ranges are also selected for satellites with other applications like Telecommunications, local Navigation and Weather Forecasting among others. LEO is further classified into Upper Low Earth Orbits, Lower Low Earth Orbits, Very Low Earth Orbits (VLEO) and Super Low Earth Orbits (SLEO), and the same is illustrated alongside orbit altitude ranges in Fig. 1.

The LEO constitutes almost 80% of the artificial satellites launched till date. As per the European Space Agency's Space Environment Report 2023, the number of satellite launches in 2022 have been more than any year before, amounting up to 2,409, majority of which were for global communications and commercial purposes [1]. This highlights the demand and growth of satellites and space-related technologies in the past few years. This has also caused a substantial increase in space traffic in LEO ranges, and potentially adds to the existing problem of orbital debris in space. It has been estimated that millions of space debris objects of varying sizes are currently in the operational orbits of the earth. The detection, tracking and mitigation of space debris has been of interest to Space Organisations like ESA and NASA, and the United Nations Committee on the Peaceful Uses of Outer Space (UN-COPOUS) published voluntary guidelines. Several technologies have been developed to address the same, and it continues to be a subject of interest within sectors of space research and development.

Recent advancements in the satellite industry include developing technologies for satellite operation in VLEO and SLEO. The interest and shift towards future satellite operations in these orbit ranges can be attributed to various reasons, including the previously discussed space debris problem. Operation in these orbit ranges proves to be more sustainable. This is because when the thruster stops operating either at End-of-Life or due to failure, the satellite deorbits and burns up in the atmosphere, not leaving space debris. Several other advantages of launching satellites in these orbits have been outlined as follows:

- reduced launch cost,
- automated demise at the end-of-life,
- reduced space debris collision risk,
- low radiation,
- payload performance advantages such as
  - increased resolution (reduced aperture size)
  - reduced antenna size

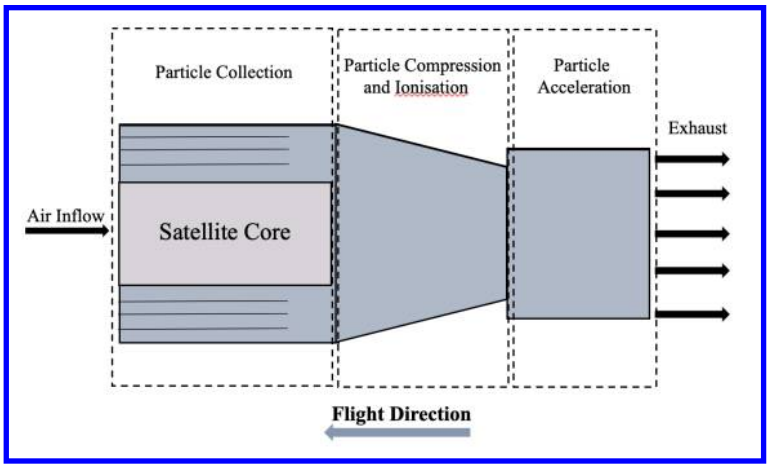

Fig. 2 General Concept and components of an ABEP system

  - transmission power
- and reduced mass- no on-board propellant and less bulky payload components

The space environment at these altitudes brings low-density atmosphere and lower solar activity. The design and operation of VLEO & SLEO satellites must consider and overcome significant challenges since this rarefied atmosphere brings added aerodynamic drag and atomic oxygen attack. When mitigation or compensation strategies for aerodynamic drag are not considered, the spacecraft in these orbits either decay rapidly or lead to de-orbit in short span of time. To increase of lifetime of such spacecraft, it is required to incorporate either traditional Electric Propulsion or use available atmosphere for air-breathing electric propulsion (ABEP) systems, where the atmospheric gas collected through intake and fed into an electric thruster for propulsion. With the traditional EP, the life of satellite can be 1-2 years, while with air-breathing operation, it can be increased to 3-8 years.

A. ABEP Concept

An Air-breathing Propulsion System uses the atmospheric air present in the orbit regions for propulsion in the engine, rather than carry it as on-board propellant. This is particularly advantageous because- 1. the mass of the spacecraft propulsion system decreases by a considerable amount, 2. the lifetime of the satellite can be increased since there is virtually unlimited supply of air (rarefied). The main components of a typical ABEP system are the intake, thruster, neutralizer and exhaust. The function of an ABEP Intake is to collect the air, compress it while keeping the flight velocity (minimal drag), and then direct it to the thruster [2]. A general configuration of an ABEP system has been illustrated in Fig. 2. As it can be seen in the figure, the efficiency of the ABEP system is highly dependent on the efficiency of the air intake in collecting sufficient air particles required for ionisation in the next stage. It must be noted that as the flow is in non-continuum regime, the external wall collisions are more present than intermolecular collisions, thus resulting in more backflow, sending the particles in the direction of flight [3]. The authors of the paper also discuss how the air particles are less obstructed by lateral structures and that long ducts with pipe-like or honeycomb-like structures (starting from the entry plane) would be more efficient than simple short ones.

Another very important point (also discussed in [3]) is the concentric design of the intake with the spacecraft core, enabling a more mass-efficient design of the air-breathing engine intake. The aerodynamic drag experienced by an air-breathing satellite can be controlled by two methods:

1) Using novel materials: To achieve specular or quasi-specular gas-surface interaction and provide atomic oxygen erosion and absorption resistance,
2) Spacecraft's geometric design: To provide efficient air-breathing, ABEP intake designs are considered as constant area [4], conical or parabolic ducts, with either honeycomb structures or smaller close-fitted ducts at the entry plane [3].

However, the perturbation in attitude of satellite can significantly reduce the gas collection efficiency for flat entry intakes e.g. 20 % reduction at 5° and 40 % reduction at 10° misalignment.

B. Past Work

In his Master's thesis on the topic of Aero-assisted Orbital Transfer Vehicles (AAOTV), McGuire et al. (2001) [5] proposed a scoop for the intake system to collect and compress incoming air particles. By conducting Direct Simulation Monte-carlo simulations to understand the associated drag values, various models for the flow conditions to calculate the drag values produced- hypersonic continuum, free molecular and transition flow are discussed. For hypersonic flow assumptions, it was suggested that a fairly tall scoop, with a high aspect ratio may be employed for efficient working, since other configurations would not be feasible for thin atmospheric conditions. The main shortcoming of the free molecular flow assumption- it theoretically limits the capture ratio of the conical inlet to 50%- is further discussed in detail. A transition flow model is proposed by the author. One of the earliest projects on the concepts of ABEP for satellites was by the Japanese Aerospace Exploration Agency, JAXA [6], in the year 2003. The design was built for an orbit altitude range between 150-200 km and included an air intake concentric with the satellite's core, a collimator for inflow with minimal backflow, and a reflector section (at an angle of 45°) to direct the particles towards the ionisation chamber. The intake incorporates a honeycomb structure to promote collisionless transmission of the particles. Further work was carried out in 2012, which validated the design concept and presented that it could successfully compress the incoming air to 0.5 Pa [7]. In 2007, following the release of the Gravity field and Ocean Circulation Explorer (GOCE) concept [8], the European Space Agency presented a RAM-EP concept [9]. The main constituents of RAM-EP were a long duct with grids at the intake to capture thin airflow, and a gridded ion engine (GIE) to generate thrust. The intake had a surface area of 0.6 m^2 and a duct length of 1 m, which provided the thruster with a steady pressure of 10^{-3} Pa. A Gridded Ion Engine (specifically, the RIT-10) was selected as the thruster based on required operational parameters and a comparison of predicted performance charts. The propellant species mixture was selected to be Oxygen (O) and Nitrogen (N_2) based on available theoretical models. In 2011, Peyret at al.[10] presented an air-breathing engine design model with a simple Hall Effect Thruster for operation in orbit altitudes of 80-110 km. The design allowed for ionisation of incoming air, which directly accelerated to the HET chamber, eliminating the need for preliminary compression. The engine was theoretically shown to effectively work between orbit altitudes 80-90 km, under the assumption that the plume is fully ionized. The authors suggest that with different geometric designs of the thruster, the same can be achieved with partial plume ionisation and at higher altitudes. In 2012, two separate studies on the topics of air-breathing propulsion were carried out. One was on ABEP designs for low orbits of Mars, conducted by BUSEK Inc. [11]. The ABEP design had an air intake of length 3.7 m, diameter 0.6 m and a honeycomb structure. The advantages of using the honeycomb structure for particle inflow was also explored in the project. The Martian Air breathing hall-Effect Thruster (MABHET) was designed to operate with Xenon. In another study [12], computational analysis of a Hall-Effect Thruster for low-earth orbit altitudes was carried out. An important finding from this study was that at an altitude of 250 km and for an oxygen and nitrogen propellant mixture, a minimum thrust of 250mN is required to overcome drag. A meticulous review of the existing technologies in LEO satellite propulsion was conducted in 2015 by Singh et al.[13]. Importantly, they discuss the work done by McGuire for his Master's thesis- DSMC analysis for a simple conical inlet for an Aero-assisted Orbital Transfer Vehicle (AAOTV). They discuss how McGuire's designs only hold for hyperthermal free molecular flow and don't have capture percentages exceeding 50%. This review paper concludes with a discussion identifying existing research gaps in the field, highlighting that concepts for aerodynamic inlets need to be further studied and analysed since the hypersonic continuum and hyperthermal flow assumptions both fall short in accurate modelling of orbit altitude atmosphere 100-120 km. In the same year, the Lanzhou Institute of Space Technology and Physics carried out a design process and feasibility analysis of an ABEP air intake device with an inlet diameter of 500 mm [14]. The device incorporated a multi-hole plate, as compared to the honeycomb structure, to reduce collisions and backflow of the particles, additionally adding three active compression devices in series- a big turbo, a small turbomolecular pump and a miniature scroll pump. The authors highlight how the compression of the fluid is difficult to achieve between orbit altitudes 150-240 km where the relative velocity is 7.8 km/s. The intake and the big turbo are analysed through DSMC computational analysis, while the turbomolecular pump and scroll pump are analysed experimentally. The authors conclude that the design achieved collection efficiency ranging from 41% and the pumps achieved a total power of 27-150 W, and that it was suitable to satisfy ABEP requirements. In 2017, an air-breathing two-stage-HET for operation at orbit altitude of 200 km and propellant mixture of pure N_2-O_2 was developed and tested at SITAEL, Italy [15]. The design RAM-EP system consisted of- a passive collector, first-stage HET for ionisation and second-stage HET for acceleration, all of which were tested at SITAEL's vacuum facility. Some important findings are- 1. a passive intake with grid-like cross-sections is the most feasible option and is capable of generating sufficient compression and collection. 2. Two-stage HET's are effective devices for air-breathing applications, given that the second stage (acceleration stage) is improved. In 2019, the von Karman Institute for Fluid Dynamics joined the RAM-EP project at SITAEL, Italy, and formed a consortium for the project, **A**ir-breathing **E**lectric

THrust**ER** (shortened AETHER). Two important findings from this study are- 1. Efficient thermal design brings the possibility of enhanced compression performance without change in collection efficiency and 2. introducing specular reflections decreases density ratio and increases the collection efficiency of an ABEP Intake. Jackson [16] discussed in the thesis at the University of Colorado the feasibility of incorporating ABEP systems in CubeSats. The author performed an analysis on three inlet shapes- a truncated pyramid, a truncated cone and a parabola, under diffuse and specular reflection conditions on the software MolFlow+. The results showed that for specular reflection, the parabolic shape had substantially higher capture percentages than the rest, while for diffuse reflection, adding baffles caused a 40% increase in the percent capture values. The DISCOVERER Project led by the University of Stuttgart and the University of Manchester introduced, tested and validated an RF Helicon-based Plasma Thruster for ABEP Systems to be operated in the VLEO [17]. The Satellite for Orbital Aerodynamics Research (SOAR) was launched in year 2021 (apogee 421 km, perigee 415km), which was a 3U CubeSat with a 9-month-lifetime-mission to collect in-situ atmospheric data like density, velocity etc. DISCOVERER is an on-going project meant to further collect and test data and methodologies for ABEP technologies, specifically on gas-surface interactions, material sciences and aerodynamic control. Zheng et al.[18] thoroughly outlined and discussed the developments up to year 2020 in the field of atmosphere-breathing propulsion systems. The authors discussed that for small satellites, passive collection and compression devices work efficiently and must be a combination of honeycomb inlet ducts, parabolic chamber with specular wall and a diffuse reflection tube. One of the most recent studies was the Direct Simulation Monte carlo simulations of JAXA's ABEP intake design using dsmcFOAM+ by Rapisarda [19]. The author proposed a thorough simulation methodology for the 3-dimensional numerical analysis of ABEP engine for an altitude of 180 km. He discussed the effects of acceleration grid transparency, intake geometry aspect ratios and intermolecular collisions among others. He also highlights the lack of accurate models for the evaluation of atmospheric conditions. Further, it was suggested that specular reflection conditions need to be thoroughly investigated since they potentially yield high collection efficiencies. Some important conclusions and inferences from literature review have been summarised as follows:

- When it comes to flow regime, most papers and studies either adopt hypersonic models or hyperthermal free molecular flow models. However, the fluid behaviour in the actual rarefied orbit environments is more complex, and more like a combination of these two. More studies need to be conducted in order to establish accurate models.
- During ABEP intake design, it must be kept in mind that small ducts/ grid instead of honeycomb structures are more efficient in providing collisionless flow with minimal backflow
- Increasing the length of the intake ducts increases the collection efficiencies (η_c)
- In general, rarefied fluid problems have often been modelled using diffuse reflection gas-surface interactions, however, the gas-surface interactions in these conditions is more complex and has specular behaviour as well. Specular and diffuse reflective properties need to be further studied to characterize a high-speed rarefied fluid problem accurately.
- Authors from most literature suggest that aerodynamic collectors cannot capture all of the oncoming flow, and this idea needs to be further investigated [13].

With the motivation to understand the effects of gas surface interaction on basic intake geometries, the current study utilizes 2-D axisymmetric numerical simulations for a hollow cylinder and convergent ducts in low-density rarefied environment. The objectives of the study are summarized as:

1) To perform time-dependent DSMC simulations using SPARTA solver developed by Sandia Laboratories [20] for basic intake geometry in VLEO/SLEO environment.
2) To develop methods for analyzing and estimating the performances of basic compression-assisted intake geometries.

II. Numerical Method

The open-source SPARTA-DSMC Simulator **S**tochastic **PA**rallel **R**arefied-gas **T**ime-accurate **A**nalyser, by Sandia Laboratories) has been used to simulate the hypersonic time-dependent cases of the test geometry cases in the low-density environments corresponding to orbital altitudes of 100, 140 and 200 km. SPARTA-DSMC uses Variable Hard Sphere model for modelling the collisions in these regimes.

A. The DSMC Technique

The Knudsen number (Kn) indicates the degree of rarefaction in a fluid flow, and can be used to determine if a certain fluid dynamics problem can be modelled using the continuum (macroscopic level) or non-continuum flow regime

(molecular level). The conventional Navier Stokes and Burnett equations provide the required accurate mathematical modelling for continuum flow regimes, but become invalid for transition and non-continuum regimes, where the tracking of macroscopic variables becomes more complex. This is where the Boltzmann equation is used, and in its general form, it is given as follows:

$$\frac{\delta f}{\delta t} + \mathbf{v} \cdot \frac{\delta f}{\delta \mathbf{r}} + \frac{\mathbf{F}}{m} \cdot \frac{\delta f}{\delta \mathbf{v}} = (\frac{\delta f}{\delta t})_{coll} \tag{1}$$

where the first term ($\frac{\delta f}{\delta t}$) represents temporal derivative, second ($\mathbf{v} \cdot \frac{\delta f}{\delta \mathbf{r}}$) and third ($\frac{\mathbf{F}}{m} \cdot \frac{\delta f}{\delta \mathbf{v}}$) terms represent convective derivatives with $\frac{\mathbf{F}}{m}$ as the density of particles in a cell, and the right-hand side term represents the time rate of change of the function due to binary collisions.

The Knudsen number is a dimensionless number, given by Eq.(2). Flow regimes with Kn < 0.001 don't experience any rarefaction effects and are characterized as no-slip continuum conditions, while flows with Kn > 10 are characterized as free molecular flows. Values between 0.1 > Kn > 0.001 characterize slip continuum conditions and between 10 > Kn > 0.1 characterize transition regime conditions.

$$Kn = \lambda / L \tag{2}$$

where λ is the mean free path and $\mathbf{L}$ is the characteristic length of the fluid problem.

Rarefied hypersonic conditions correspond to non-continuum flows, for which the Boltzmann equation is solved using various deterministic (Discrete Velocity Models (DVM), Fourier spectral method) and stochastic (Monte-carlo methods) approaches. The Direct Simulation Monte Carlo can model realistic and computationally efficient simulations for dilute gases while resolving the mathematical complexities that the multidimensional and collisional structure of the Boltzmann equation brings.

B. Initial and Boundary Conditions

For the simulations, three orbit altitudes in the VLEO ranges have been considered- 100 km, 140 km and 200 km. Using the orbital speed equation for a circular orbit (Eq. (3)), the freestream velocities at each of these altitudes were calculated, which were then used to calculate the remaining required input parameters as tabulated in Table 1.

$$v = \sqrt{\frac{GM}{r}} \tag{3}$$

where G is the gravitational constant (equal to $5.97 \times 10^{-11}\ N - m^2/kg^2$), M is the mass of the earth and r is the radius of the orbit.

The gas-surface interactions between the incoming flow particles and surface of the intake geometry determines the drag on the surface, by giving an idea of the heat and momentum transfer between them. The factor to model the type of gas-surface interactions is defined as the accommodation coefficient (denoted by α, Eq. 4), which is equal to 0 for ideal specular and 1 for ideal diffuse reflections.

$$\alpha = \frac{E_i - E_r}{E_i - E_w} \tag{4}$$

where E_i is the mean kinetic energy of incident particles, E_r is the kinetic energy of the reflected particles and E_w is the mean energy corresponding to the wall temperature. Rarefied flows are modelled using diffuse gas-surface interactions [21], however, the authors also highlight that experimental data does not align with this assumption. In [16], the authors discuss that for satellites, quasi-specular reflections take place due to adsorption taking place on the surface. As more contaminants are adsorbed on the surface, the gas-surface interactions experience more diffuse reflections. Therefore, for the current study, simulations were run for both diffuse and specular reflections, with α of 0 and 0.95 for realistic specular and diffuse type of gas-surface interactions respectively.

C. Geometry Cases

First, three basic configurations, namely, a hollow cylinder, a convergent-divergent section and a divergent-convergent section were analysed for orbit altitude conditions of 200 km. This was done to understand the behaviour of the fluid around constant-area and varying-area ducts. After assessing these initial simulation results, it was inferred that a combination of a constant-area section with a convergent section would yield better particle collection.

Table 1 Freestream conditions for (i) orbit altitude 100 km, (ii) 140 km and (iii) 200 km

Parameters	Values at each altitude		
	Case (i)	Case (ii)	Case (iii)
Freestream Mach Number (M_∞)	27.63	15.34	11.92
Free-stream Velocity (v_∞, kg/m^3)	7844.2	7820.1	7784.3
Free-stream Density (ρ_∞, kg/m^3)	5.583×10^{-7}	3.854×10^{-9}	3.284×10^{-10}
Free-stream Temperature (T_∞, K)	194	625	1026
Free-stream Pressure (p_∞, Pa)	0.03214	0.00071	0.0001
Free-stream Number Density (n_∞, $/m^3$)	1.2001×10^{19}	8.2864×10^{16}	7.0594×10^{15}
Wall Temperature (T_w, K)	300	300	300
Mean free path (λ_∞, m)	0.113	16.391	192.398

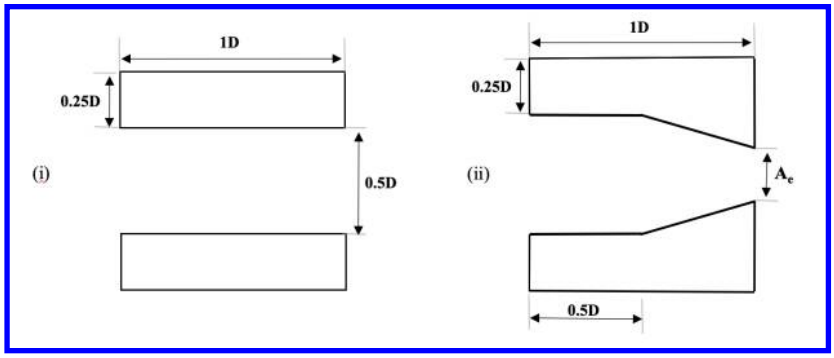

Fig. 3 Dimensions of (i) Reference geometry and (ii) straight-convergent geometric configuration

Therefore, three geometries incorporating ducts with constant-area section followed by a converging section were analysed, with different outlet areas- 0.1 m^2, 0.2 m^2 and 0.3 m^2. These outlet areas result in convergent angles of 68.2°, 73.3° and 78.7° respectively. The hollow cylinder geometry case was considered as the reference geometry and was then run for the remaining altitudes of 100 km and 140 km.

All of the geometries tested had a diameter D = 1 m, length L = D and thickness t = 0.25D. The inlet diameters for all the tested geometry is 0.5D. The rest of the paper discusses dimensions in terms of the diameter D. Fig. 3 shows the selected geometry. (i) shows the hollow cylinder used in preliminary simulations, and (ii) shows the configuration of the three main test geometries. The term A_e represents the exit area and takes values 0.1, 0.2 and 0.3 for each of the cases.

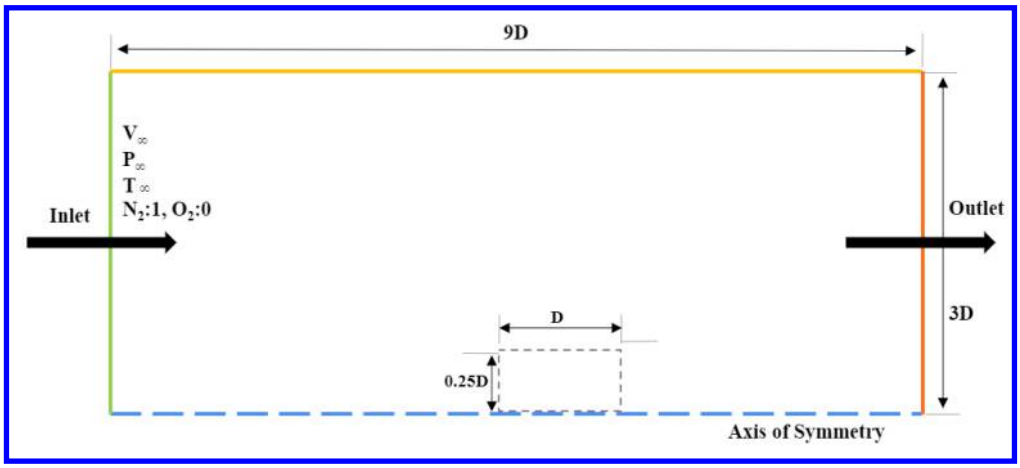

Fig. 4 Computational Domain

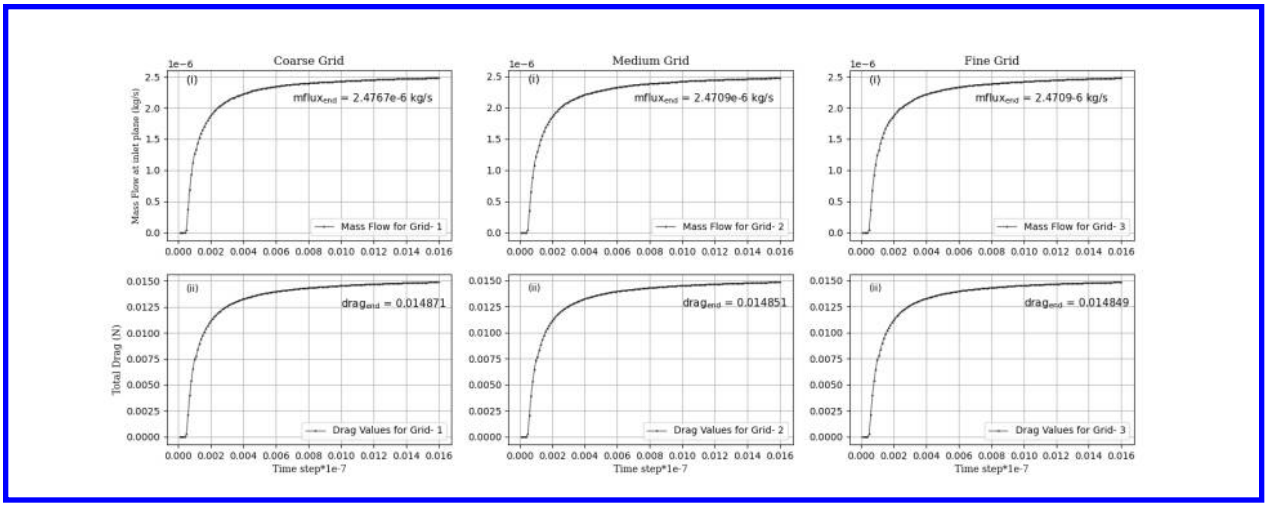

Fig. 5 Plots for the three grids for (i) Mass Flux values at the inlet plane and (ii) Drag values

D. Computational Domain and Grid Independence

The computational domain for simulation must be big enough such that the resultant output parameter results remain unaffected by the boundaries, and only purely dependent on the equations and initial conditions. 2-dimensional axisymmetric numerical simulations, with a computational domain of the size 9D × 3D have been run. The selected test geometries were simulated with boundary conditions and computational domain as illustrated in Fig. 4. The small dotted rectangle in the centre represents the location of the test geometries, all of which have an inlet diameter of 0.25D (as shown in figure). The selected computational domain allows for efficient capture of downstream flow as well.

Initially, a subjective assessment of the grid resolution was done based on some preliminary validation cases. However, [22] was consulted and simulations were run for a coarse grid (Grid size = 250 × 100), a medium grid (Grid size = 300 × 120) and a fine grid (Grid size = 360 × 140). The results were analysed for the values of inlet mass flux and drag values with respect to time, and graphs for the same have been plotted (Fig. 5. It can be noted that for grids 2 and 3, the values of mass flux don't change up to 5 significant digits and up to 4 for drag coefficient values. Since the computational power and time is greater for grid 3, grid 2 was chosen for final simulations.

III. Results and Discussions

Before the numerical simulations of the three main geometric configurations were performed, a preliminary run for three basic configurations (paragraph 1 of II.C) was carried out first in order to validate the solver and establish an understanding of varying duct cross-sectional areas. As mentioned in subsection II.C, the hollow cylinder geometry is the reference case for the main simulations, and has also been analysed for collection efficiency. The collection efficiencies and drag coefficient values are calculated for each of the geometries in the 2D axisymmetric analysis. The collection efficiency (η_c) is defined as follows:

$$\eta_c = \frac{m_{flux}}{\rho_\infty v_\infty} \tag{5}$$

The drag coefficient (c_D) is defined as follows:

$$c_D = \frac{F_D}{0.5\rho_\infty (v_\infty)^2 S} \tag{6}$$

A. Flow Field Analysis

The contour plots for number density in flow field of the three convergent geometries can be seen in Fig. 6. The columns represent the three different geometries, (a) is Geometry-1, (b) is Geometry-2 and (c) is Geometry-3. Each of the rows represents different altitude conditions- Row-1 is 100 km, Row 2 is 140 km and Row-3 is 200 km. It can be seen that in the wake of the three test geometries, there is a significant variation for each of the cases (i.e., specular and

diffuse reflections at three different orbital altitudes). In the wake region of the diffuse cases, the particle number density is well-distributed and higher in comparison to specular conditions at each altitude. It can also be seen from the figure that shock waves are more pronounced in specular reflection cases, which is expected since diffuse reflection causes more dispersion. These shock waves are more prevelant at higher altitudes of 140 km and 200 km, causing an increase in the drag experienced by the geometry at these cases. For the diffuse cases, the particles are also denser between the convergent section.

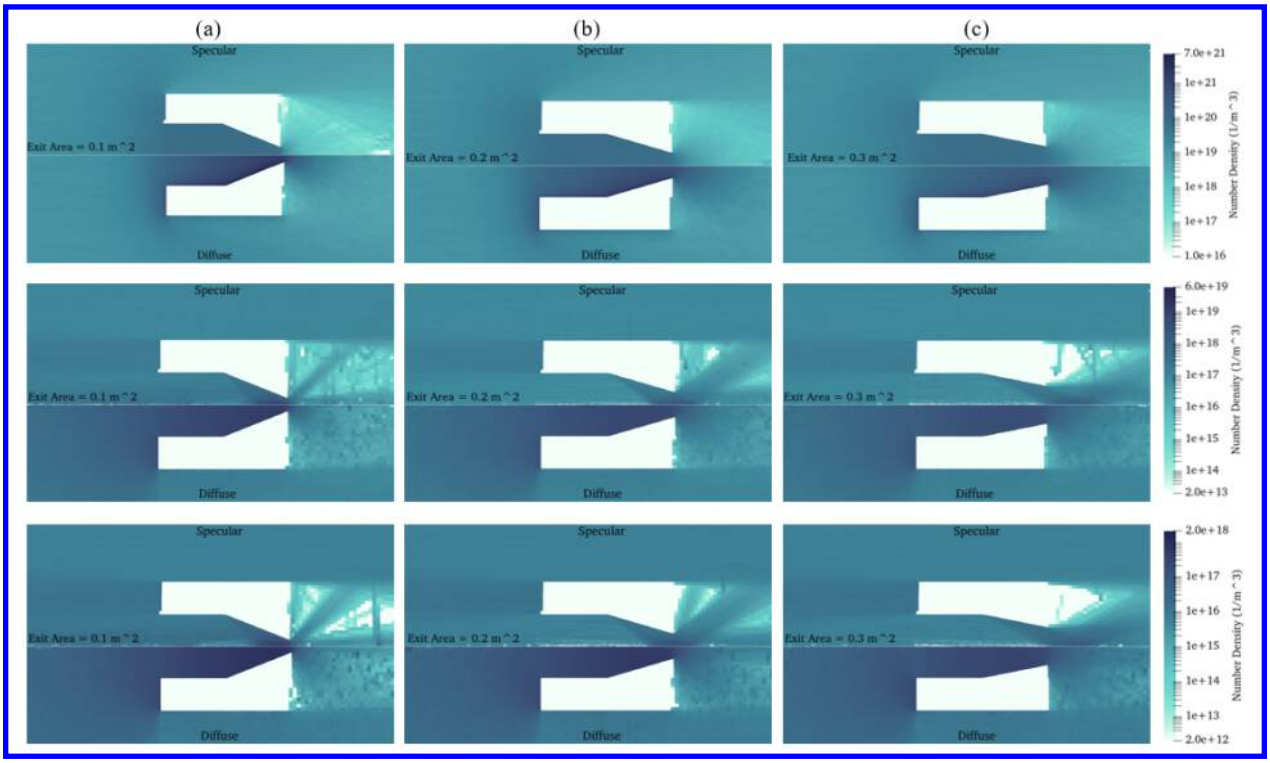

Fig. 6 Contours for number density values at 100 km (Row 1) altitude, 140 km (Row 2) altitude and 200 km (Row 3) altitude

B. Collection Efficiencies and Drag

The reference case, i.e., hollow cylinder geometry, was analysed for specular and diffuse reflection conditions for the three selected altitudes. A comparison of the resultant collection efficiencies for each altitude have been illustrated in Fig. 7. It can be seen that at the lower altitude of 100 km, the collection efficiencies show bigger difference between specular and diffuse cases, while with increase in altitude (to 200 km), the difference in collection efficiencies decreases as the collection efficiency for diffuse reflection reduces. The collection efficiencies and drag coefficients for all the three geometries as well as reference geometry (hollow cylinder) at different altitudes has been plotted against the timestep, as can be seen in Fig. 8. The continuous lines represent diffuse reflection cases while the dashed lines represent the results for specular reflection cases. With increase in simulation timestep, the output parameters reach a constant value and the collection of incoming flow is established in the given geometries. Similar to the trend observed in the hollow cylinder, the difference in collection efficiency values for diffuse and specular cases are prominent at 100 km, and almost negligible at the higher altitude of 200 km. Again, the values for diffuse cases are very high at 100 km, and reduce with increase in altitude. As expected from the number density flow field analysis done in subsection III.A, the drag coefficients for specular cases are quite high at 140 and 200 km. The final values of collection efficiencies and drag coefficients have also been also tabulated in Table 2. The table highlights how diffuse reflection conditions have considerable reduction of collection efficiencies with increase in altitude, while no such trend is observed in case of specular reflection. At 200 km, the collection efficiencies under both, specular and diffuse reflection conditions seem to be the same, at about 96%. Collection efficiencies greater than 100% have been observed for diffuse reflection cases at altitudes 100 km and 140 km. On the other hand, the drag coefficient values for specular cases increase by a

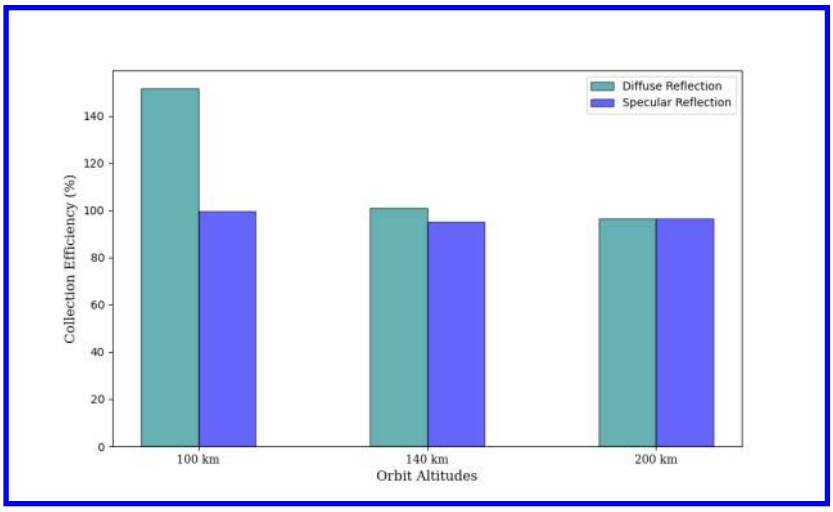

Fig. 7 Collection Efficiency values for reference hollow cylinder geometry

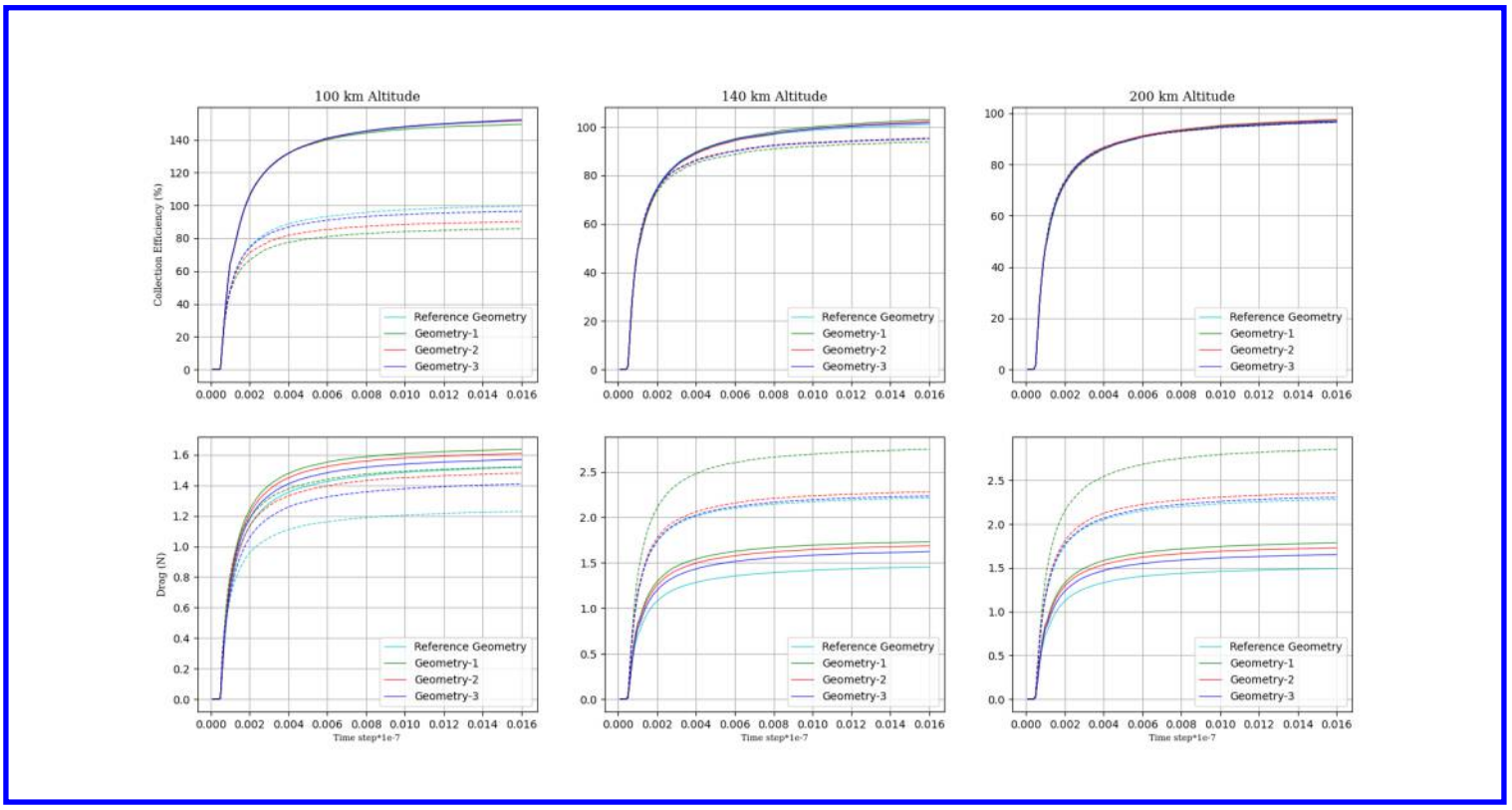

Fig. 8 Resultant plots for the three geometric configurations

considerable amount with increase in altitude, and the same trend follows for all the geometry cases, while this trend is not observed in diffuse reflection cases.

IV. Conclusions and Future Work

All of the simulations and analysis in this paper were for two-dimensional axisymmetric geometries in hypersonic rarefied flow at different altitudes of 100 km, 140 km and 200 km. The predicted mass flow rates, reflected in collection efficiencies, are affected by exit areas as well as gas-surface interactions. However, these dependencies are more complex,

Table 2 Collection efficiencies and drag coefficients for the geometries under diffuse and specular cases

Geometry		100 km		140 km		200 km	
		η_C	C_D	η_C	C_D	η_C	C_D
Reference Geometry: Hollow Cylinder	Diffuse	151.66 %	1.518	101.10 %	1.454	96.66 %	1.492
	Specular	99.66 %	1.229	95.21 %	2.213	96.67 %	2.282
Geometry-1: Exit Area 0.1 m^2	Diffuse	149.46 %	1.635	102.98 %	1.731	97.33 %	1.785
	Specular	85.85 %	1.521	93.77 %	2.748	96.49 %	2.853
Geometry-2: Exit Area 0.2 m^2	Diffuse	151.83 %	1.607	102.21 %	1.687	97.50 %	1.729
	Specular	90.10 %	1.479	95.30 %	2.278	96.40 %	2.355
Geometry-3: Exit Area 0.3 m^2	Diffuse	152.32 %	1.569	101.71 %	1.623	96.85 %	1.652
	Specular	96.43 %	1.409	95.10 %	2.233	96.57 %	2.306

and require more study and analysis to arrive at any conclusive trends. With increase in altitude (and consequently rarefaction), there is a considerable decrease in the collection efficiencies under diffuse reflection conditions, and a considerable increase of drag coefficients under specular reflection conditions. A similar general trend for the drag coefficients under diffuse reflection conditions and for collection efficiencies under specular reflection conditions was not observed.

The future work for this research involves performing 3-dimensional numerical simulations to further understand the collection efficiencies with values higher than 100%. As also inferred from the literature, the effect of diffuse and specular reflections needs to be further investigated. The current study shows that the collection efficiencies are lower under specular conditions than for under diffuse conditions, and this trend does not hold for higher altitudes of 200 km. Additionally, the geometry must be further optimized by including the thermal effects, yielding more conclusive results and help establishing trends.

Acknowledgments

The authors wish to acknowledge Irish Research Council Postgraduate Scholarship (under grant number GOIPG/2022/1832) for providing the financial support to carry out current research.

References

[1] Office, E. S. D., "ESA's Annual Space Environment Report," Tech. rep., European Space Angency, 2023.

[2] Zheng, P., Wu, J., Zhang, Y., and Wu, B., "A Comprehensive Review of Atmosphere-Breathing Electric Propulsion Systems," *International Journal of Aerospace Engineering, Hindawi*, Vol. 2020, 2020, p. 8811847. https://doi.org/10.1155/2020/8811847.

[3] Romano, F., Espinosa-Orozco, J., Pfeiffer, M., Herdrich, G., Crisp, N., Roberts, P., Holmes, B., Edmondson, S., Haigh, S., Livadiotti, S., Macario-Rojas, A., Oiko, V., Sinpetru, L., Smith, K., Becedas, J., Sulliotti-Linner, V., Bisgaard, M., Christensen, S., Hanessian, V., Jensen, T. K., Nielsen, J., Chan, Y.-A., Fasoulas, S., Traub, C., García-Almiñana, D., Rodríguez-Donaire, S., Sureda, M., Kataria, D., Belkouchi, B., Conte, A., Seminari, S., and Villain, R., "Intake design for an Atmosphere-Breathing Electric Propulsion System (ABEP)," *Acta Astronautica*, Vol. 187, 2021, pp. 225–235. https://doi.org/https://doi.org/10.1016/j.actaastro.2021.06.033.

[4] Rapisarda, C., "Modelling and simulation of atmosphere-breathing electric propulsion intakes via direct simulation Monte Carlo," *CEAS Space Journa*, Vol. 1400, 2021. https://doi.org/10.1007/s12567-021-00414-z.

[5] Mcguire, T. J., "Aero-assisted Orbital Transfer Vehicles Utilizing Atmosphere Ingestion," Master's thesis, Massachusetts Insitute of Technology, 2001.

[6] *Air breathing ion engine concept*, Bremen, germany, 2003.

[7] Hisamoto, Y., Nishiyama, K., and Kuninaka, H., "Design of air intake for air breathing ION engine," *Proceedings of the International Astronautical Congress, IAC*, Vol. 9, 2012, pp. 7630–7634.

[8] Johannessen, J., Balmino, G., Provost, C. L., Rummel, R., Sabadini, R., Sunkel, H., Tscherning, C., Visser, P., Woodworth, P., Hughes, C., Pascal, L. G., Sneeuw, N., Perosanz, F., Fernandez, M. A., Rebhan, H., and Drinkwater, M., "The European Gravity Field and Steady-State Ocean Circulation Explorer Satellite Mission: Its impact on geophysics," *Surveys in Geophysics*, Vol. 24, No. 4, 2003, pp. 339–386. https://doi.org/https://doi.org/10.1023/B:GEOP.0000004264.04667.5e, URL https://archimer.ifremer.fr/doc/00000/493/.

[9] Peyret, R., and Taylor, T. D., *RAM Electric Propulsion for low earth orbit operation: an ESA study*, Florence, Italy, 2007.

[10] Pekker, L., and Keidar, M., "Analysis of Air Breathing Hall Effect Thruster," 2011. URL https://api.semanticscholar.org/CorpusID:122761059.

[11] Hohman, K., Investigator, P., and Circle, T., "ATMOSPHERIC BREATHING ELECTRIC THRUSTER FOR PLANETARY EXPLORATION," 2012. URL https://api.semanticscholar.org/CorpusID:124721736.

[12] Garrigues, L., "Computational Study of Hall-Effect Thruster with Ambient Atmospheric Gas as Propellant," *Journal of Propulsion and Power*, Vol. 28, No. 2, 2012, pp. 344–354. https://doi.org/10.2514/1.B34307, URL https://doi.org/10.2514/1.B34307.

[13] Singh, L. A., and Walker, M. L., "A review of research in low earth orbit propellant collection," *Progress in Aerospace Sciences*, Vol. 75, 2015, pp. 15–25. https://doi.org/https://doi.org/10.1016/j.paerosci.2015.03.001, URL https://www.sciencedirect.com/science/article/pii/S0376042115000226.

[14] Li, Y., Chen, X., Li, D., Xiao, Y., Dai, P., and Gong, C., "Design and analysis of vacuum air-intake device used in air-breathing electric propulsion," *Vacuum*, Vol. 120, 2015, pp. 89–95. https://doi.org/https://doi.org/10.1016/j.vacuum.2015.06.011, URL https://www.sciencedirect.com/science/article/pii/S0042207X15002730.

[15] Andreussi, T., Cifali, G., Giannetti, V., Piragino, A., Ferrato, E., Rossodivita, A., Andrenucci, M., Longo, J., and Walpot, L., "Development and Experimental Validation of a Hall Effect Thruster RAM-EP Concept," 2017.

[16] Jackson, S. W., and Marshall, R., "Conceptual Design of an Air-Breathing Electric Thruster for CubeSat Applications," *Journal of Spacecraft and Rockets*, Vol. 55, No. 3, 2018, pp. 632–639. https://doi.org/10.2514/1.A33993, URL https://doi.org/10.2514/1.A33993.

[17] Roberts, P., Crisp, N., Edmondson, S., Macario Rojas, A., Smith, K., Mcgrath, C., Haigh, S., Oiko, V., Holmes, B., Sinpetru, L., and et al., "DISCOVERER: Final Results and Outcomes," *73rd International Astronautical Congress*, 2022. 73rd International Astronautical Congress, IAC 2022 ; Conference date: 18-09-2022 Through 22-09-2022.

[18] Zheng, P., Wu, J., Zhang, Y., and Wu, B., "A Comprehensive Review of Atmosphere-Breathing Electric Propulsion Systems," *International Journal of Aerospace Engineering*, Vol. 2020, 2020. https://doi.org/10.1155/2020/8811847.

[19] Rapisarda, C., "Modelling and simulation of atmosphere-breathing electric propulsion intakes via direct simulation Monte Carlo," *CEAS Space Journal*, Vol. 15, 2023. https://doi.org/10.1007/s12567-021-00414-z, URL https://doi.org/10.1007/s12567-021-00414-z.

[20] https://sparta.github.io/, ???? SPARTA DSMC Simulator by Sandia Laboratories.

[21] Sharipov, F., and Barreto, Y. B., "Influence of gas–surface interaction on gaseous transmission probability through conical and spherical ducts," *Vacuum*, Vol. 121, 2015, pp. 22–25. https://doi.org/https://doi.org/10.1016/j.vacuum.2015.07.015, URL https://www.sciencedirect.com/science/article/pii/S0042207X15300191.

[22] Lee, M., Park, G., Park, C., and Kim, C., "Improvement of Grid Independence Test for Computational Fluid Dynamics Model of Building Based on Grid Resolution," *Advances in Civil Engineering*, 2020. https://doi.org/10.1155/2020/8827936.